Supporting Information for

2D-Organic Framework Confined Metal Single Atoms with the Loading Reaching the Theoretical Limit

Chao Lin,[a, b] Hao Zhang,[c] Xiaokai Song,[d] Dong-Hyung Kim,[b] Xiaopeng Li,[*a] Zheng Jiang,[*c, e] Jung-Ho Lee[*b]

[a] State Key Laboratory for Modification of Chemical Fibers and Polymer Materials & College of Materials Science and Engineering, Donghua University, Shanghai 201620, China. E-mail: xiaopeng.li@dhu.edu.cn

[b] Department of Materials Science and Chemical Engineering, Hanyang University, Ansan, Gyeonggi-do, 15588, Korea. E-mail: jungho@hanyang.ac.kr

[c] Shanghai Synchrotron Radiation Facility, Zhangjiang Lab, Shanghai Advanced Research Institute (SARI), Chinese Academy of Sciences (CAS), Shanghai 201210, China. E-mail: jiangzheng@sinap.ac.cn

[d] School of Chemical & Environmental Engineering, Jiangsu University of Technology, Changzhou 213001, China

[e] Shanghai Institute of Applied Physics, Chinese Academy of Science, Shanghai 201800, China

Experimental Section:

Chemicals: $CoCl_2 \cdot 6H_2O$, $NiCl_2 \cdot 6H_2O$, $FeCl_3 \cdot 6H_2O$, $MnCl_2 \cdot 4H_2O$, $RuCl_2 \cdot 2H_2O$, chloranilic acid, ethylenediamine, 1-methy-2-pyrolidinone (NMP) and 5 wt% Nafion solution were purchased from Sigma-Aldrich. Commercial 20 wt% PtRu/C obtained from Alfa Aesar. Commercial 20 wt% Pt/C was purchased from Johnson Matthey.

Synthesis of hexaaminobenzene (HAB): Typically, 0.5 g of chloranilic acid was mixed with 5 g of ethylenediamine in 15 mL of NMP, followed by addition of a few drops of sulfuric acid with vigorous stirring in an ice bath for 5 min. The resultant solution was brought to room temperature before a heat treatment at 80 °C for 12 h to ensure complete amination of the chloranilic acid. The resulting solid product was collected by vacuum filtration, washed with degassed ethanol and diethyl ether, and then freeze dried for 24 h to afford the brownish-black hexaaminobenzene complex.

Synthesis of cobalt hexaaminobenzene intermediate (Co-HAB): Hexaaminobenzene (1.18 mmol) was added into a dry 100 mL beaker with 45 mL of DI water and several drops of ammonia under an air atmosphere. After stirring at room temperature for 1 h, 45 mL of a DI $CoCl_2$ solution (157.3 mmol/L) was poured into the mixture solution. After stirring for at least another 2 h, the resulting precipitate was collected by centrifugal separation. After washing with DI water (at least five times to remove impurities), the intermediate (used for synthesis of Co/C_2N-H) was freeze dried for 24 h to remove residual H_2O. The concentration of $CoCl_2$ was changed to 13.1 mmol/L to obtain intermediates for synthesis of Co/C_2N-L.

Synthesis of single-atom-cobalt-incorporated C_2N (Co/C_2N-L and Co/C_2N-H): 100 mg of Co-HAB was first dissolved in 7.5 mL of anhydrous NMP in an ice bath, and then 7.5 mL of NMP with 120 mg of chloranilic acid was added with vigorous stirring at room temperature. After adding a few drops of ethylenediamine and sulfuric acid, the resulting solutions were

heated at 120 °C for 8 h and then cooled to room temperature. The product was subsequently washed with methanol and deionized water at least three times, followed by freeze drying for 24 h. Finally, the obtained brown powders were annealed at 300 °C for 30 min under N_2 at a ramping rate of 2 °C min^{-1} to yield Co/C_2N-H. To obtain 2-D nanosheets, as-prepared Co/C_2N-H was dispersed in a mixture of isopropanol and H_2O (v/v = 3/2), followed by sonication for 24 h. After separating the precipitate, the upper supernatant was freeze dried for another 24 h.

Synthesis of Ni/C_2N, Fe/C_2N, CoFe/C_2N, and CoMn/C_2N: Ni/C_2N, Fe/C_2N, CoFe/C_2N, and CoMn/C_2N can be obtained by the same method as Co/C_2N, except the metal precursor is different. For example, $NiCl_2 \cdot 6H_2O$ (7.07 mmol) was used for Ni/C_2N, $FeCl_3 \cdot 6H_2O$ (7.07 mmol) for Fe/C_2N, $FeCl_3 \cdot 6H_2O$ (3.53 mmol) and $CoCl_2 \cdot 6H_2O$ (3.53 mmol) for CoFe/C_2N, and $MnCl_2 \cdot 4H_2O$ (3.53 mmol) and $CoCl_2 \cdot 6H_2O$ (3.53 mmol) for CoMn/C_2N.

Synthesis of RuO_2: Ruthenium (III) chloride (1 mM) was well dissolved into solutions of methyl alcohol and water (1:1 v/v) under vigorous stirring. Then, the pH of solution was adjusted to 7 by dropwise 2M sodium hydroxide solution. The precipitate was centrifuged, rinsed with deionized water, and dehydrated for 80 °C, followed by annealing for 500 °C for 5 h in the air.

Characterization. Powder XRD was performed with a Rigaku D/MAX-2500 diffractometer with Cu Kα radiation (λ = 1.5406 Å) at a scan rate of 2° min^{-1} under an operating voltage of 40 kV and current of 100 mA. Nitrogen desorption/adsorption measurements were carried out using an AUTOSORB-1-MP system at 77 K. Before the N_2 adsorption experiment, the samples (~50 mg) were activated by drying them in a vacuum at 120 °C for 5 h. The pore size distribution was determined by Barrett-Joyner-Halenda (BJH) methods. Atomic force microscopy (AFM) images were obtained using an XE-100 microscope. All the experiments were measured under ambient conditions. TGA data for all samples were obtained by an SDT Q600 thermal

gravimetric analyzer (Auto-DSCQ20 system) from room temperature to 900 °C with a ramping rate of 10 °C/min under air. The inductively coupled plasma optical emission spectrometry (ICP-OES) was conducted on Thermo Fisher ICAP 7000SERIES. The morphology and structure were analyzed by a JEOL-6700F field-emission scanning electron microscope (FE-SEM). A JEOL JEM-2010F transmission electron microscope was used to obtain TEM images and EDS mapping results. To realize the atomic structure, aberration-corrected scanning transmission electron microscopy (AC-STEM) images were acquired on a double spherical aberration-corrected STEM (JEM-ARM200F). X-ray photoelectron spectroscopy (XPS) was carried out with a VG SCIENTA (R 3000) spectrometer. The X-ray absorption spectroscopy (XAS) measurements were obtained on the Beam line BL14W1 at the Shanghai Synchrotron Radiation Facility (SSRF) with a double Si (111) crystal monochromator and the electron storage ring operated at 3.5 GeV. The linear combination fitting (LCF) for valence analysis were performed using the ATHENA software package.

Electrochemical measurements. All electrochemical analyses were conducted using a CHI 760 D electrochemical workstation (CHI, Inc., USA) with a three-electrode system including a catalyst-loaded glassy carbon pine rotating disk electrode (0.19625 cm^{-2}), a Pt wire, and Ag/AgCl with saturated KCl as the working electrode, counter electrode, and reference electrode, respectively. O_2-saturated 0.1 M KOH was used as the electrolyte with O_2 bubbling maintained during ORR experiments. Typically, 5 mg of the catalyst, 5 mg of carbon black, and 70 μL of Nafion (5 wt.%) were dispersed in isopropyl alcohol (0.6 mL) by sonication for 2 h to form a homogeneous ink. Then, 14 μL of this catalyst ink was coated on the cleaned glassy carbon to make the prepared catalysts. Linear sweep voltammetry (LSV) was carried out at rotation speed of 1600 rpm with a scan rate of 10 mV s^{-1}. The OER measurements were performed in a typical three-electrode system that contains a working electrode (i.e. glassy carbon electrode), a graphite rod counter electrode, and an Ag/AgCl (saturated KCl solution)

reference electrode. The electrolyte is 1 M KOH electrolyte saturated with Argon. The KOH electrolyte was purified according to a previously reported method.[1] The work electrode preparation method is the same as that applied in the ORR measurement. Linear sweep voltammetry (LSV) curves were recorded at a rotation speed of 1600 rpm with a scanning rate of 5 mV s^{-1}. All the LSV curves were corrected with 95% iR-compensation. The R is the ohmic drop determined using the impedance measurements. The potential was obtained based on the equation $E = E_{recorded} - iR$. The $E_{recorded}$ is the recorded potential (vs. RHE). All the current densities were calculated using the geometrical surface area of the electrodes.

Zn-air flow battery measurement. A homemade battery cell was used to perform the ZAFB performance measurement. The air cathodes were prepared by uniformly coating the same homogenous catalyst ink on a carbon paper with backside coated with gas-diffusion layer. The preparation was reported in our previous paper.[2] The catalyst loading was controlled around 1 mg cm^{-2}. A polished Zn plate was used as the anode. The rechargeable ZABs used a solution of 6 M KOH with 0.2 M zinc acetate as electrolyte.

Computational details. The density functional theory (DFT) calculations were performed using the Vienna Ab initio Simulation Package (VASP)[3] with the projector augmented-wave (PAW) method to describe the ion-electron interaction.[4] Electron exchange-correlation was represented by the functional of the generalized gradient approximation in the Perdew, Burke, and Ernzerhof form (GGA-PBE).[5] The convergence threshold was 10^{-5} eV and 0.01 eV/Å for energy and force, respectively. The cutoff of energy was set to 500 eV for all calculations. The Brillouin zone was sampled by a 3*3*1 Monkhorst-Pack k-point mesh.[6] A vacuum layer of at least 15 Å was applied in the z-direction of the slab models to prevent vertical interactions between slabs. The van der Waals (vdW) dispersion was considered by employing the D3 method of Grimme.[7]

Theoretical mass loading calculation. If the Co single atoms completely filled all of the hole in C_2N frameworks, each structural unit contains of one cobalt atom, twelve carbon atoms and six nitrogen atoms. The cobalt mass loading of Co_1/C_2N can be governed by Equation S1:

$$L_{Co}(wt.\%) = \frac{n_{Co} \times M_{Co}}{\sum_{i=C,N,Co} n_i \times M_i}$$

S1

Where n_{Co}, n_N, n_C are the atomic number of Co, N, C in one structural unit, which equal to 1, 6, and 12, respectively, in Co_1/C_2N. the M_i represents the molar mass of corresponding element. The theroretical maxium cobalt mass loading of Co_1/C_2N calculated using equation S1 are 20.53 wt.%. And the maxium cobalt mass loading of Co_2/C_2N, and Co_3/C_2N can be determined as 41.06 wt.%, and 61.59 wt. %, respectively, when the n_{Co} equal to 2 and 3, respectively.

Figures
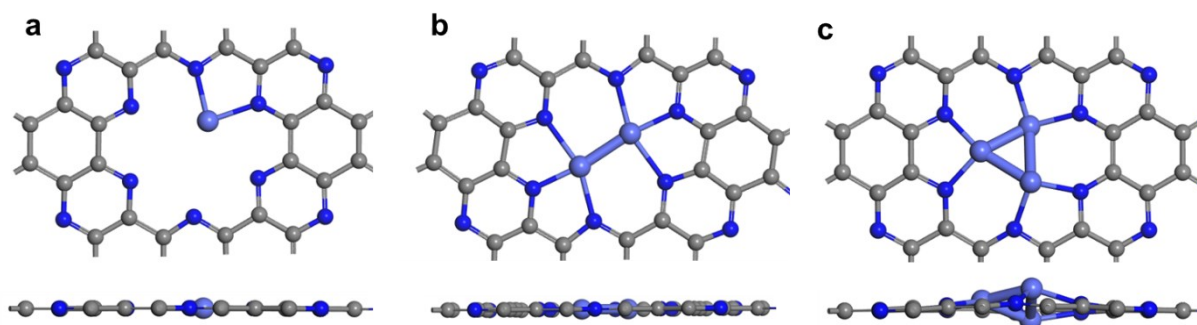
Figure S1. Top view and side view of the structures of Co-N-hole in (a) Co_1/C_2N, (b) Co_2/C_2N, and (c) Co_3/C_2N.
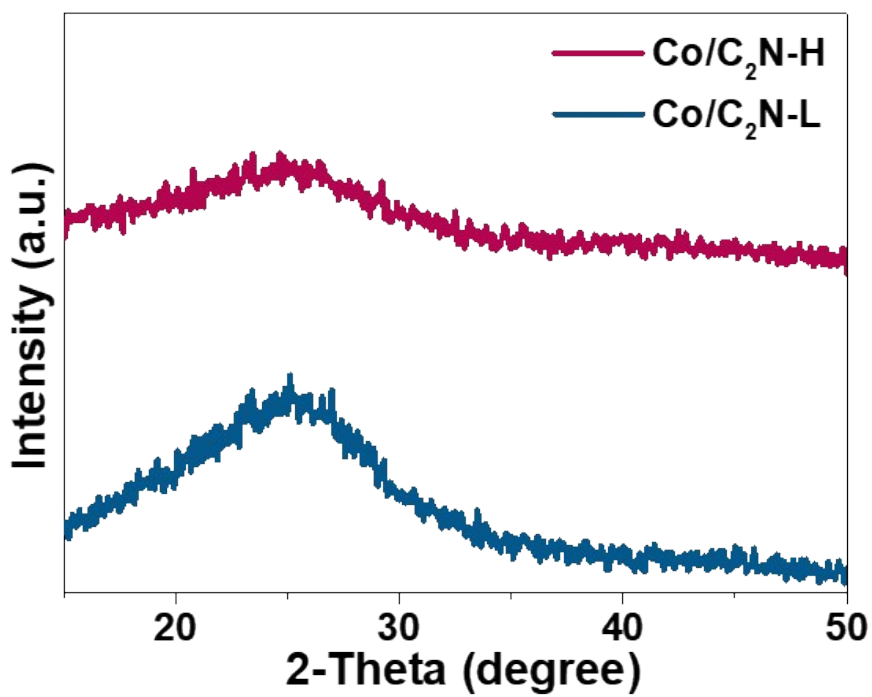
Figure S2. XRD patterns for Co/C_2N-L and Co/C_2N-H.
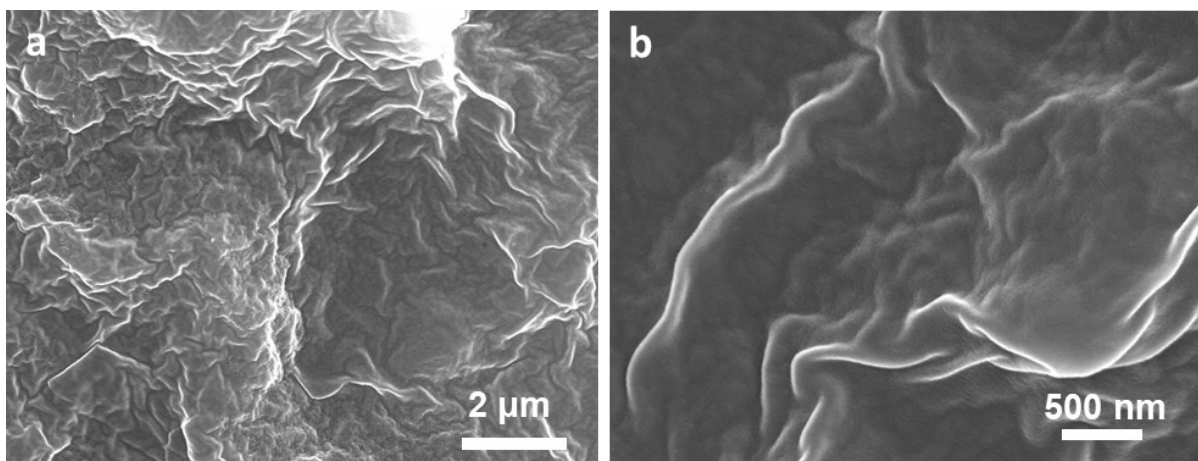
Figure S3. SEM images of C$_2$N nanosheets after sonication.
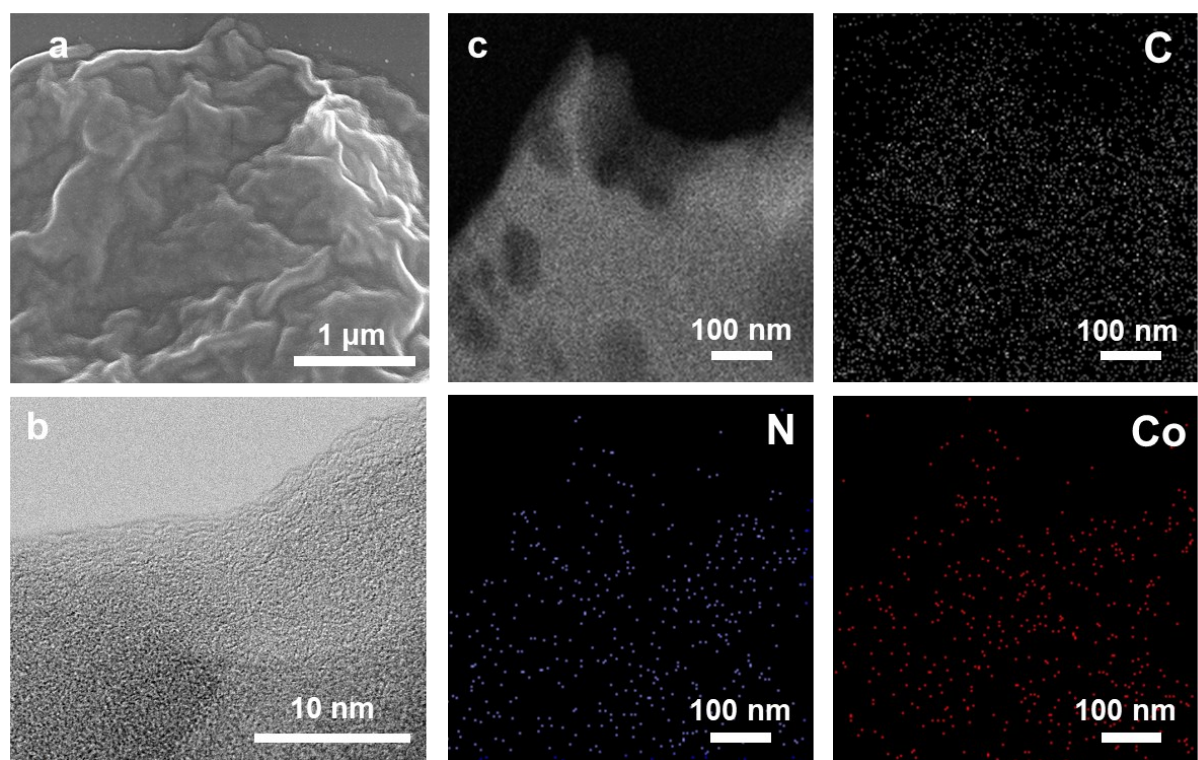
Figure S4. a) SEM, b) TEM, and c) STEM images of Co/C$_2$N-L with corresponding EDS mapping results.
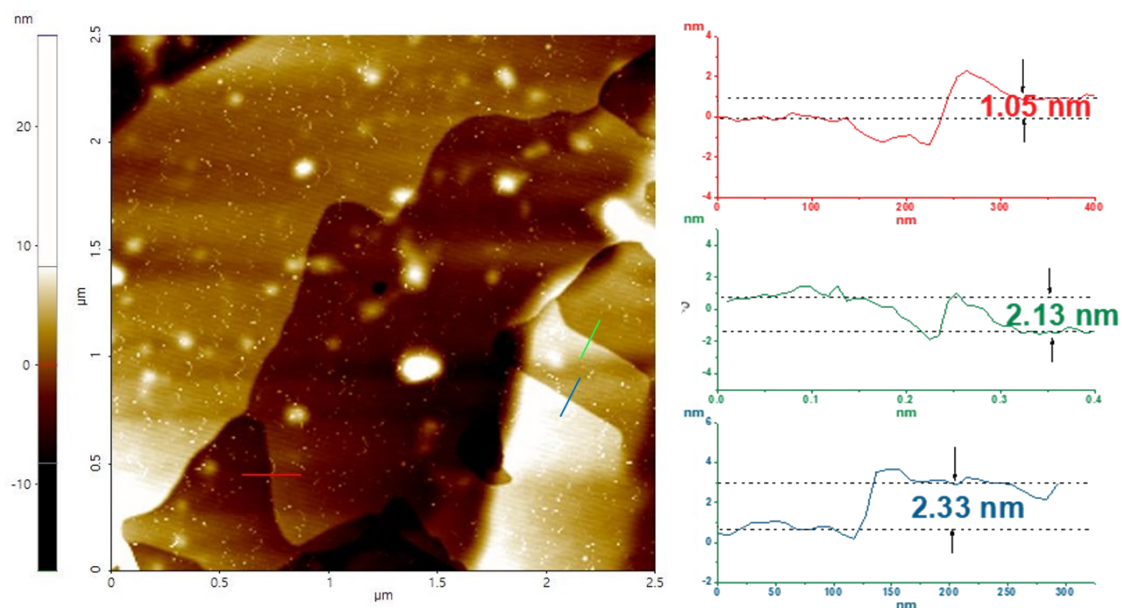
Figure S5. AFM image and corresponding height profiles of Co/C$_2$N-H. The white circular spots caused by the ambient noise during the test.
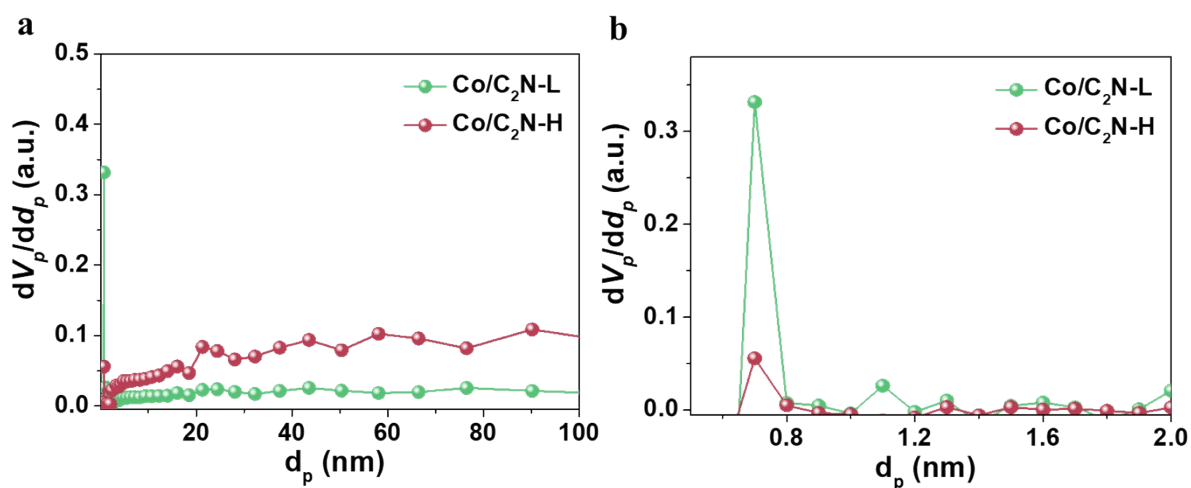
Figure S6. (a) pore size distribution curve of Co/C$_2$N-L and Co/C$_2$N-H. (b) is the magnified view of (a).
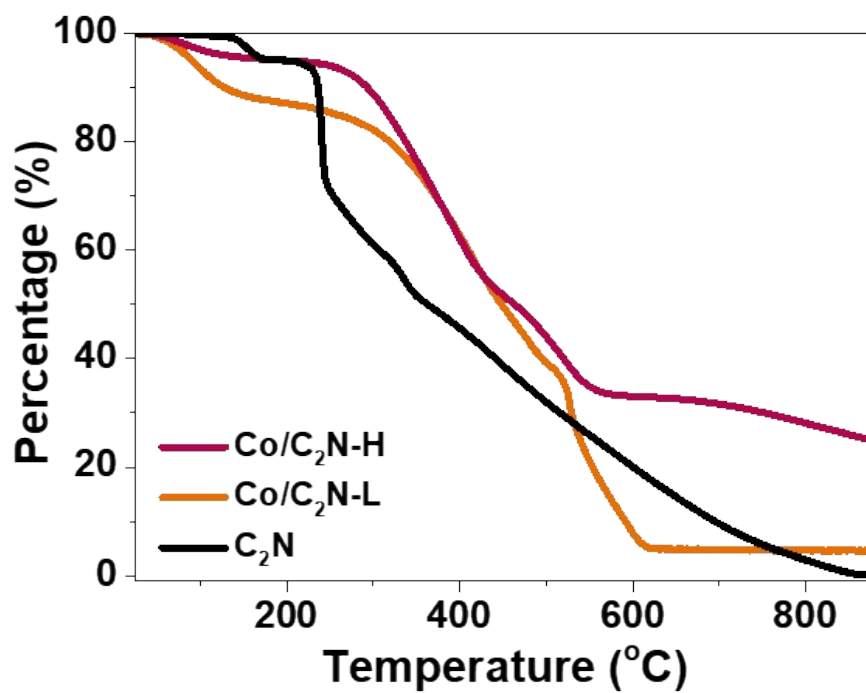
Figure S7. Thermogravimetric analysis results obtained with a heating rate of 10 ^{o}C/min in air.
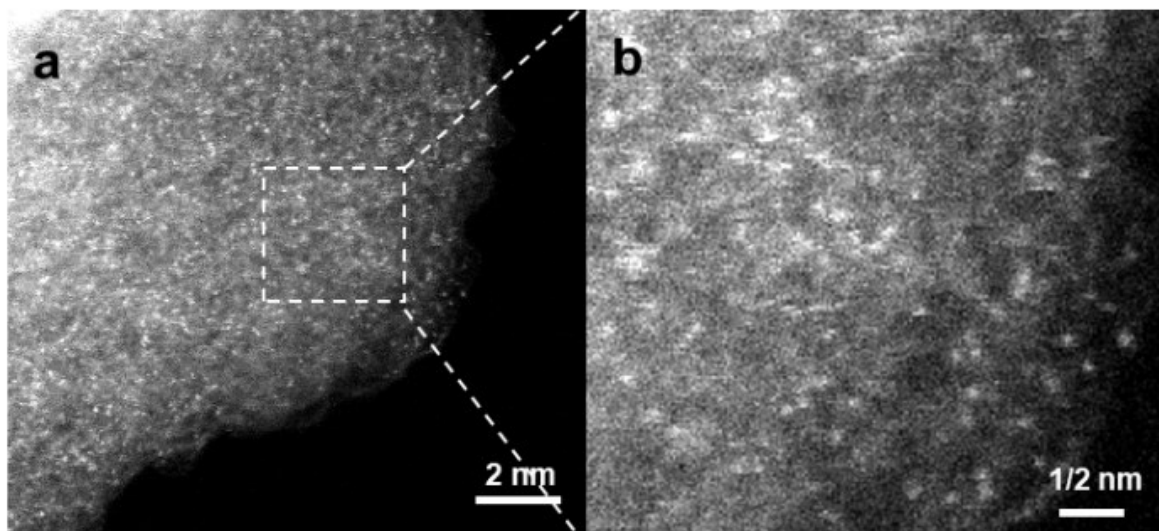
Figure S8. AC HAADF-STEM images of Co/C$_2$N-L.
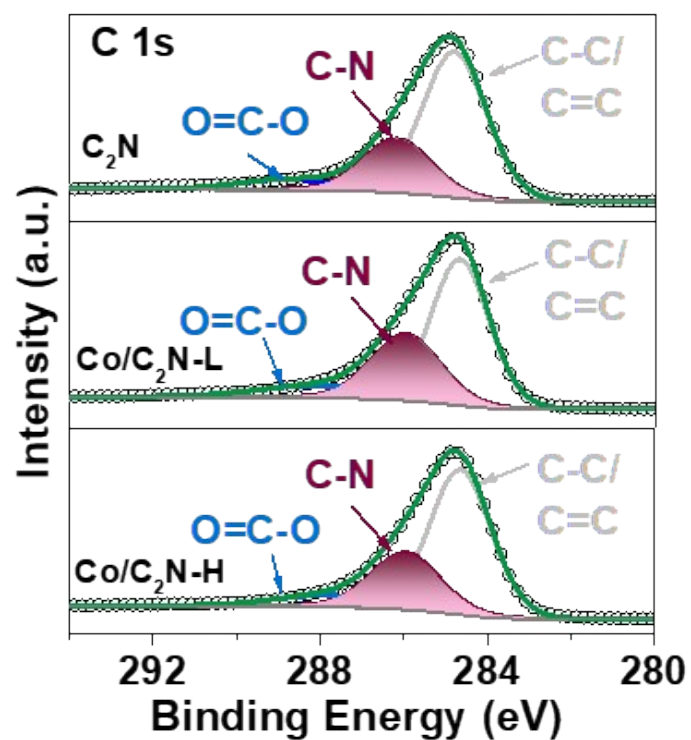
Figure S9. High-resolution C 1s spectra of C_2N, Co/C_2N-L, and Co/C_2N-H.
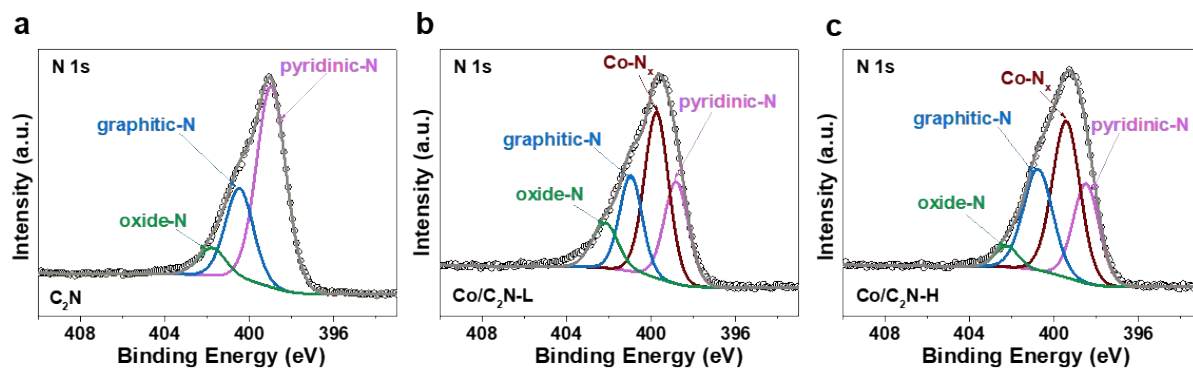
Figure S10. High-resolution N 1s spectra of C_2N, Co/C_2N-L, and Co/C_2N-H.
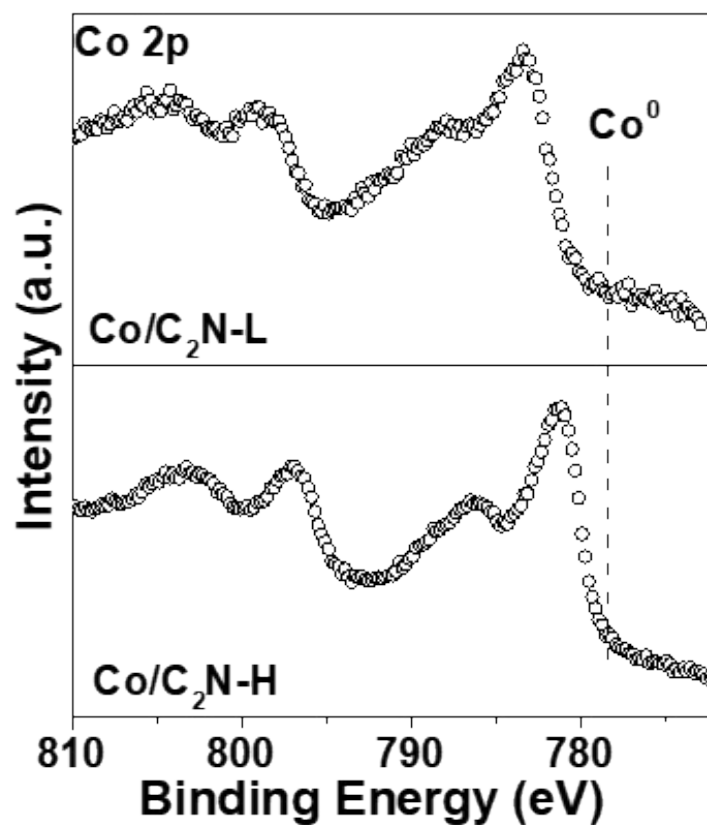
Figure S11. High-resolution Co 2p spectra of Co/C$_2$N-L, and Co/C$_2$N-H.
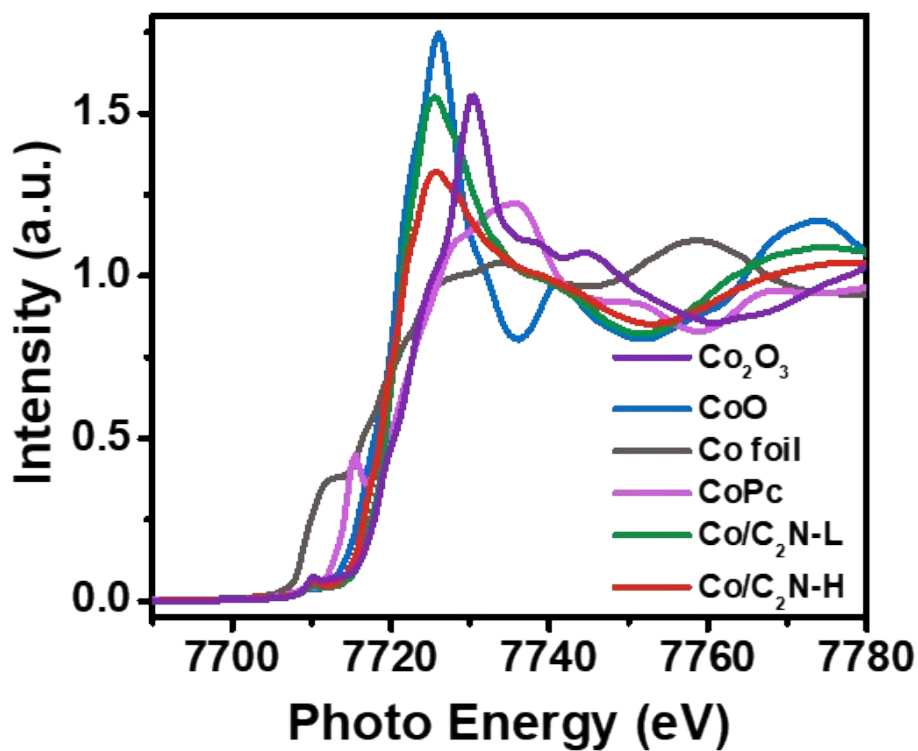
Figure S12. XANES spectra of Co/C$_2$N-H, Co/C$_2$N-L, and reference samples including Co foil, CoO, CoPc, and Co$_2$O$_3$.
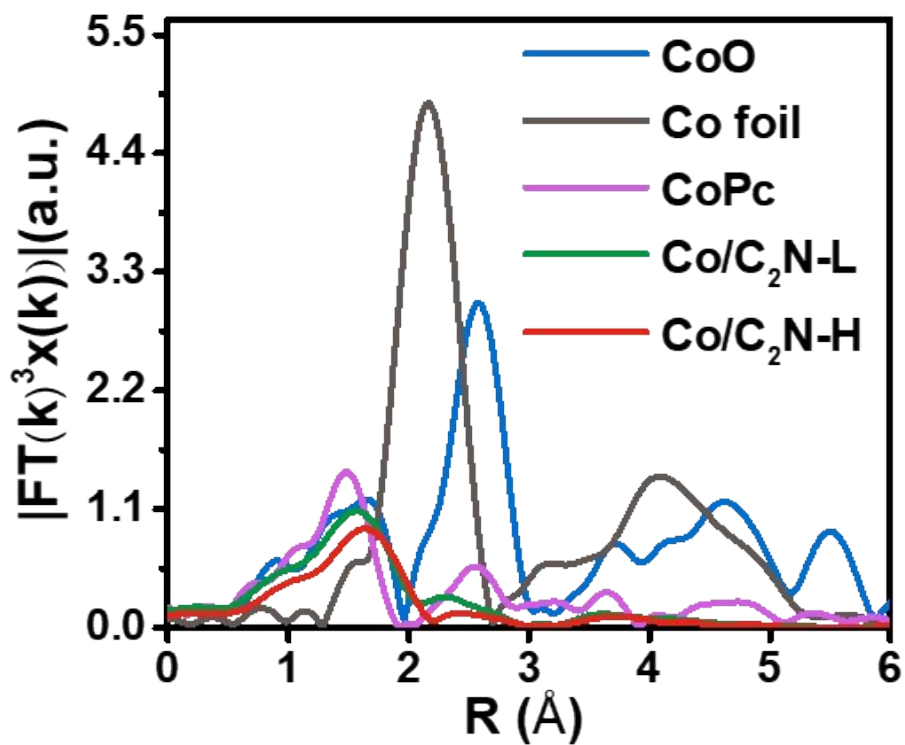
Figure S13. Co EXAFS curves of Co foil, CoO, CoPc, Co/C_2N-L and Co/C_2N-H.
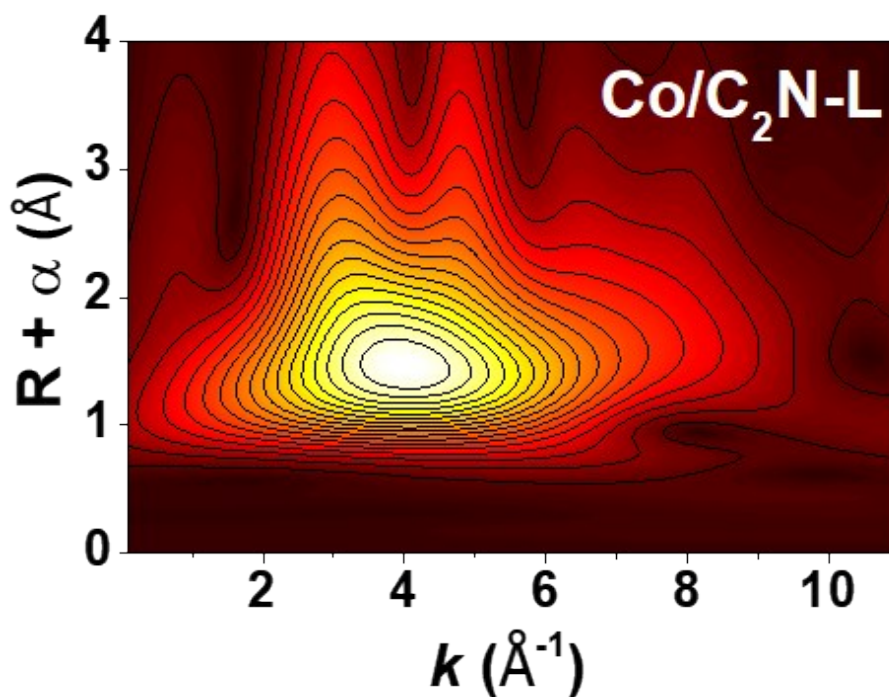
Figure S14. Wavelet transforms for k^2-weighted $\chi(k)$ Co K-edge EXAFS signals of Co/C_2N-L.
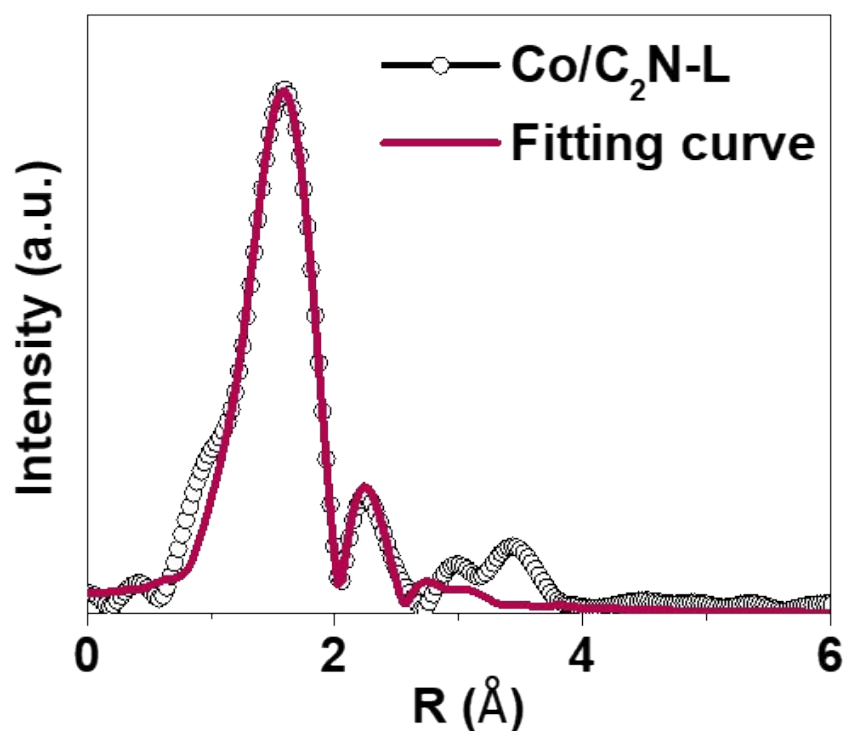
Figure S15. Co EXAFS spectrum of Co/C$_2$N-L with a corresponding fitting curve.
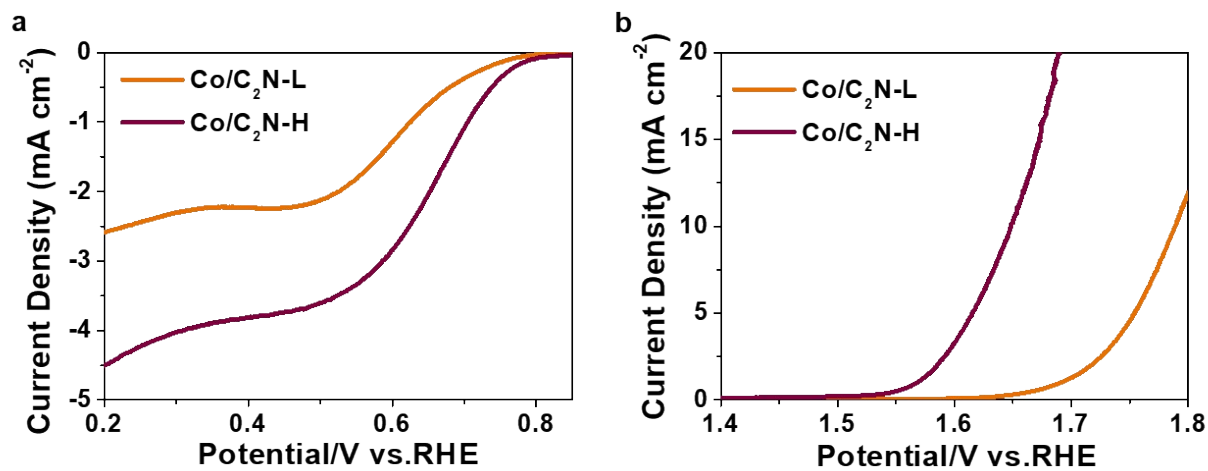
Figure S16. (a) ORR and (b) OER LSV curves of Co/C$_2$N-L and Co/C$_2$N-H with a scan rate of 10 mV s^{-1} and a rotation speed of 1600 rpm.
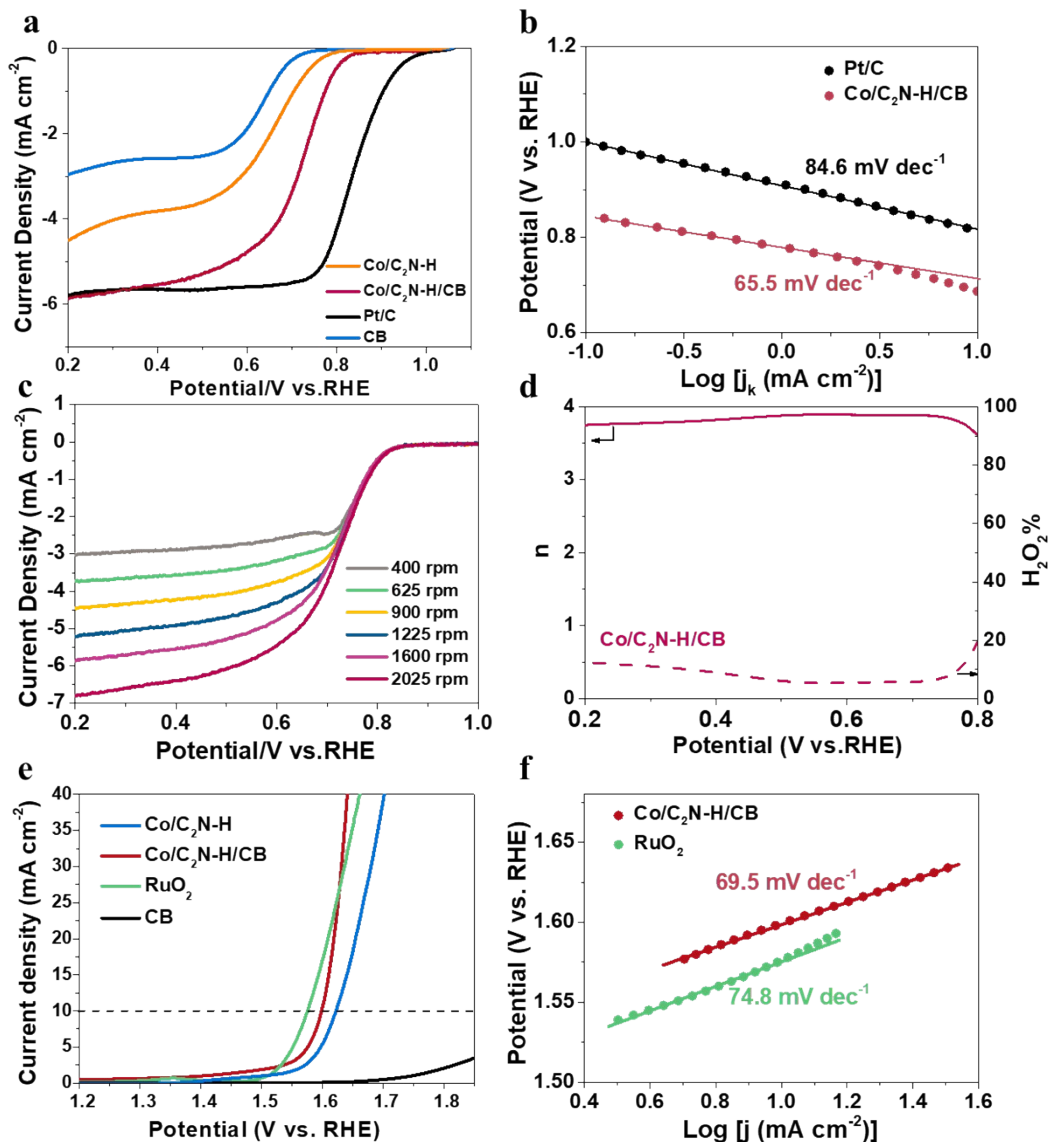
Figure S17. (a) ORR LSV curves of pristine Co/C$_2$N-H, Co/C$_2$N-H/CB with CB and Pt/C as reference samples, at a scan rate of 10 mV s^{-1} and a rotation speed of 1600 rpm. (b) Tafel slope of Co/C$_2$N-H/CB and Pt/C obtained from the corresponding LSV curves for ORR. (c) LSV curves of Co/C$_2$N-H/CB obtained at different rotating rate in the region of 400 rpm to 2025 rpm. (d) Electron transfer number with corresponding H$_2$O$_2$ yield of Co/C$_2$N-H/CB during ORR process. (e) OER LSV curves of pristine Co/C$_2$N-H, Co/C$_2$N-H/CB with CB, and RuO$_2$ as reference samples in 1 M KOH. (f) Tafel slope of Co/C$_2$N-H/CB and RuO$_2$ obtained from the corresponding LSV curves for OER.

15

a

Discharge

e^- e^-

e^- e^-

Charge

Electrode

Candidate electrolyte: lead, benzoquinone, bromine, vanadium ...

Membrane

Zn anode

Conventional Zn-based flow air battery   Pump

b

Discharge

e^- e^-

e^- e^-

Charge

O_2

Air cathode

Electrolyte: Aqueous KOH

Zn anode

O_2

O_2

Zinc dendrite growth

Conventional Zn air battery

c

Discharge

e^- e^-

e^- e^-

Charge

O_2

Air cathode

Electrolyte: Aqueous KOH

Zn anode

O_2

O_2

Mitigated Zinc dendrite growth

Zn air flow battery   Pump

Figure S18. Schematically illustration of various batteries structure including: (a) Conventional Zn based flow battery, (b) Conventional Zn air battery, and (c) Zn air flow battery.
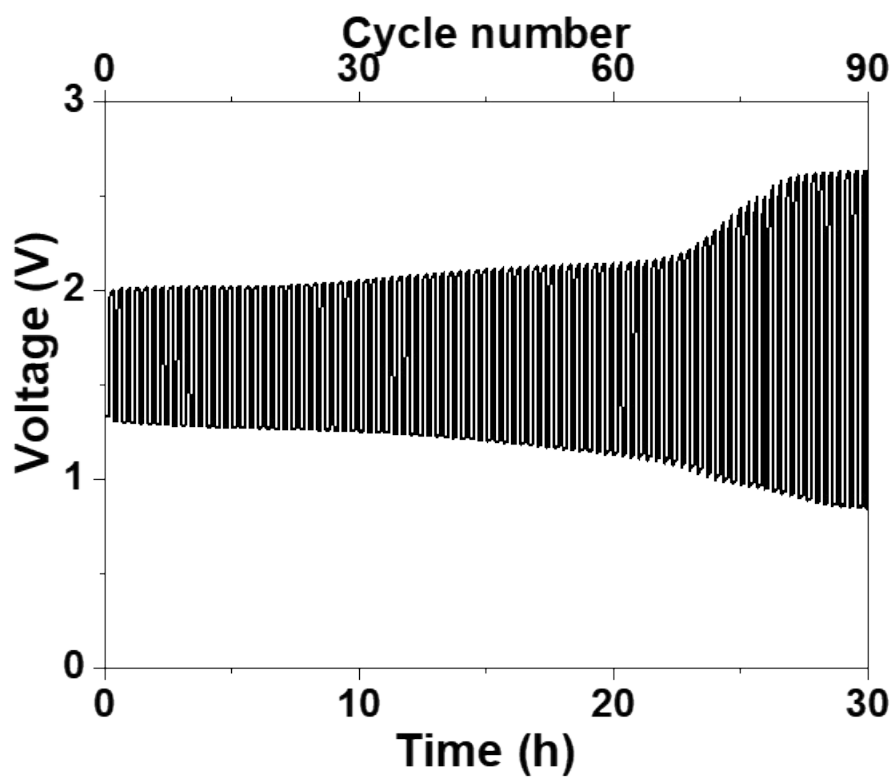
Figure S19. Galvanostatic cycling profile of PtRu/C-based ZAFB.
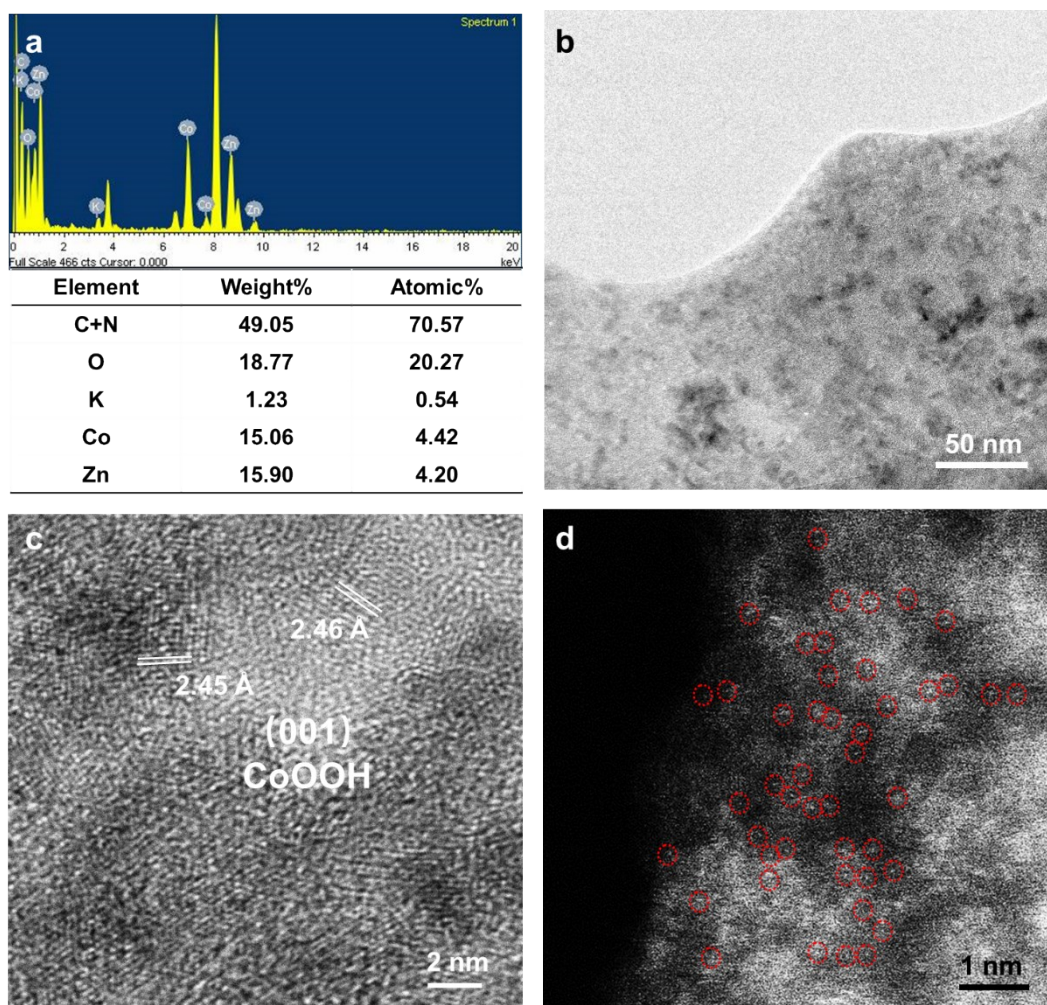
Figure S20. (a) EDS analysis data, (b, c) TEM images, (d) AC HAADF-STEM image of Co/C$_2$N-H after long-term galvanostatic cycling measurement. The K and Zn elements as shown in EDS results may originate from the electrolyte residue (e.g., KOH) and discharge byproducts (e.g., ZnO) adsorbed at the electrocatalyst surface. Note: The EDS signal of C and N overlapped together.

Element	Weight%	Atomic%
C+N	49.05	70.57
O	18.77	20.27
K	1.23	0.54
Co	15.06	4.42
Zn	15.90	4.20
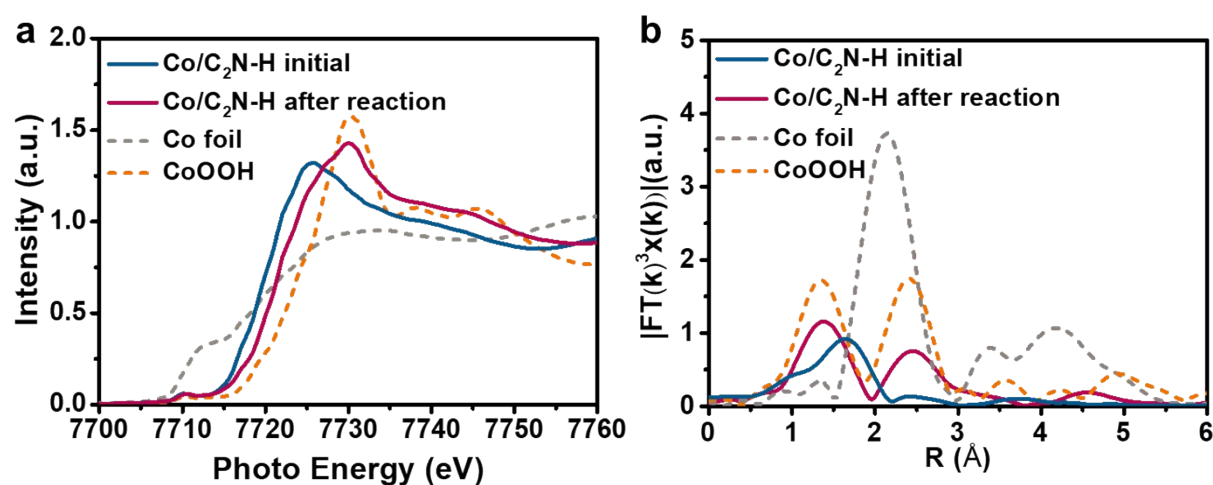
Figure S21. (a) Co K-edge XANES and (b) EXAFS spectra of Co/C$_2$N-H before and after cycling measurements with the Co foil, and CoOOH as reference samples.

18
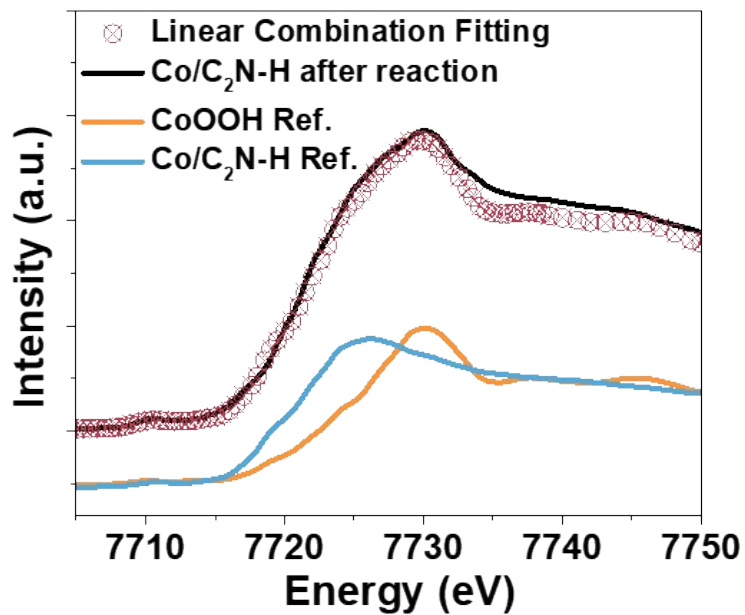
Figure S22. Valence analysis of Co K-edge XANES of Co/C$_2$N-H after cycling measurement. Linear combination fitting result reveals the relative content of Co-N$_2$ (53 %), and CoOOH (47 %).
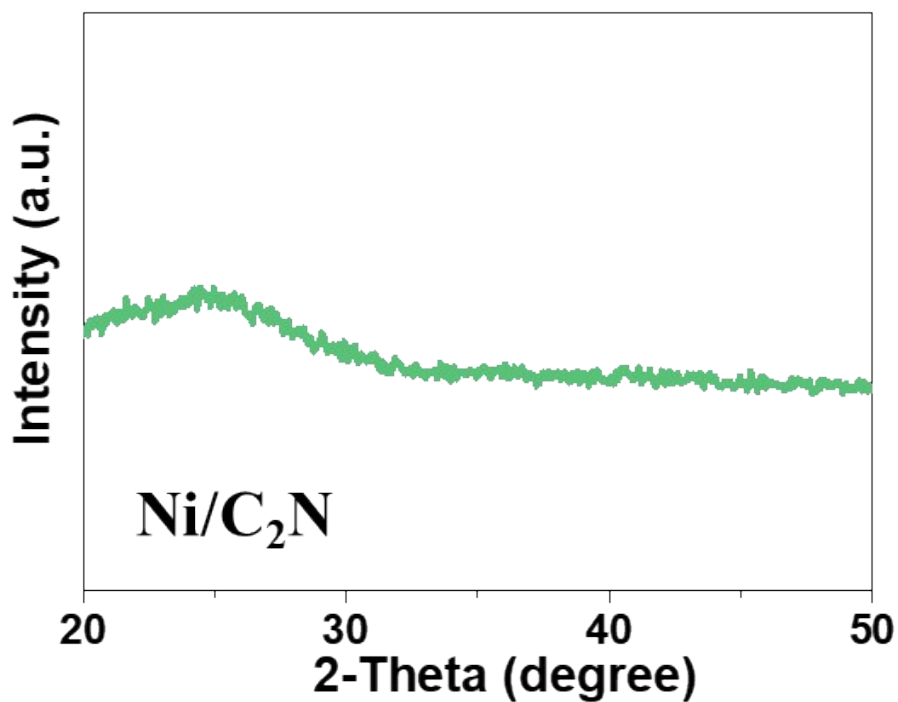
Figure S23. XRD pattern of Ni/C$_2$N.
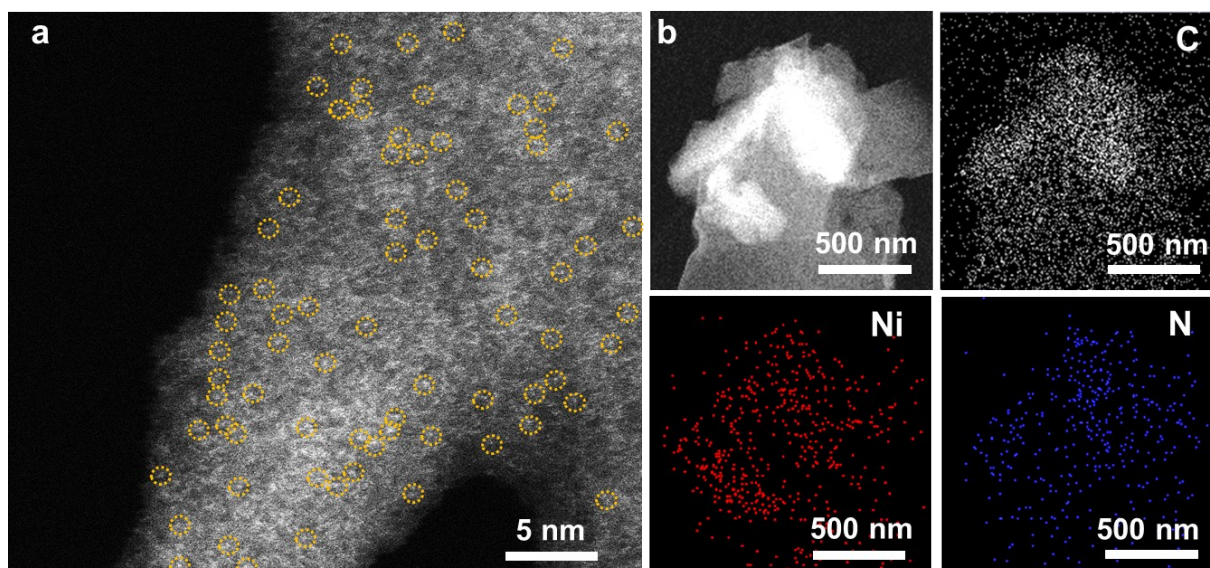
Figure S24. (a) AC HAADF-STEM image and (b) EDS mapping data of Ni/C$_2$N.
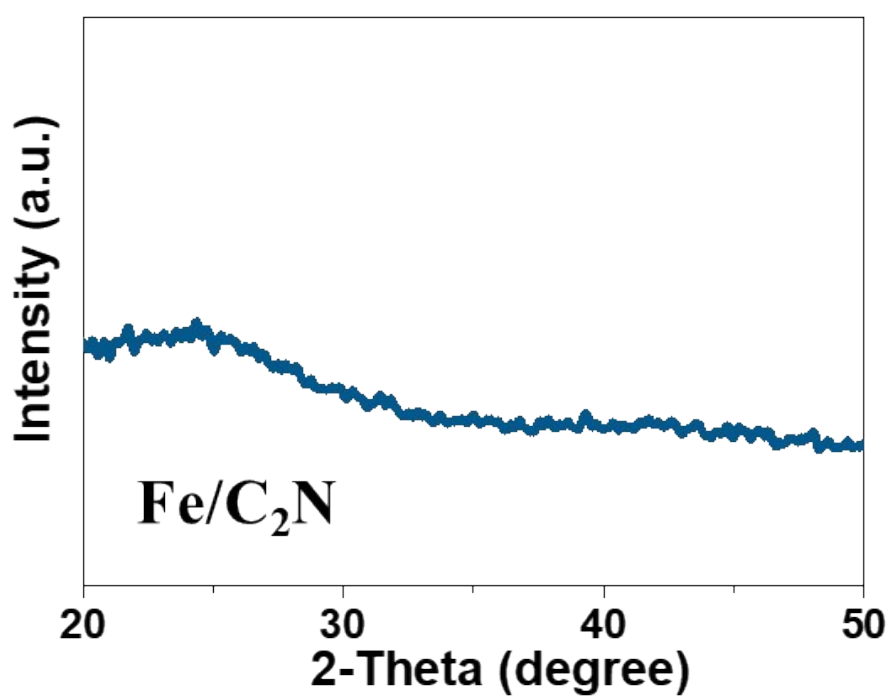
Figure S25. XRD pattern of Fe/C$_2$N.
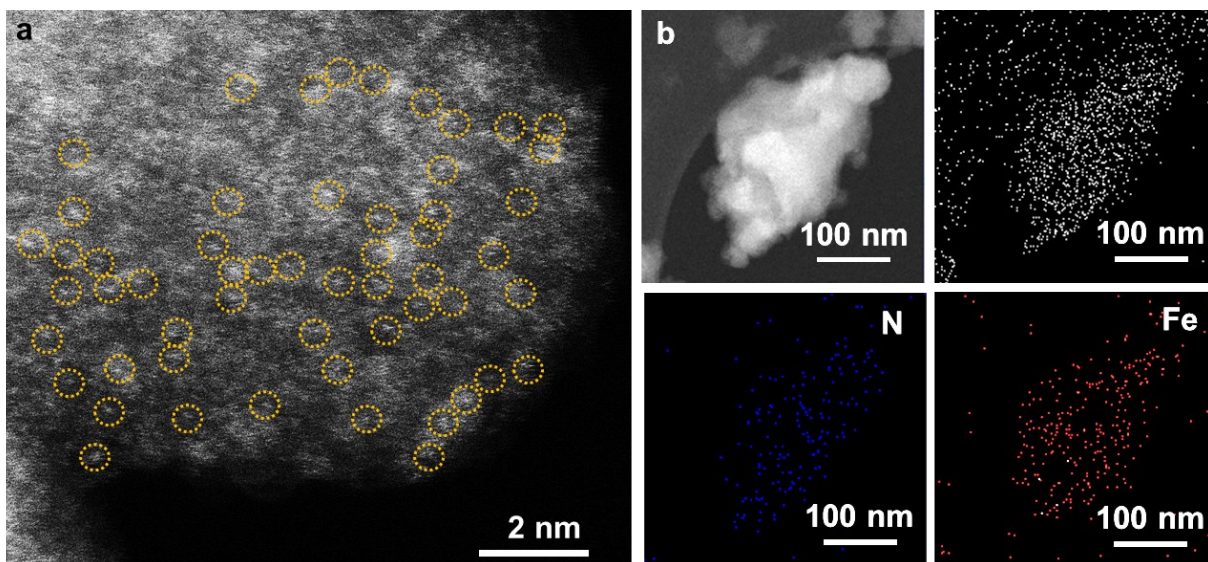
Figure S26. (a) AC HAADF-STEM image and (b) EDS mapping data of Fe/C$_2$N.
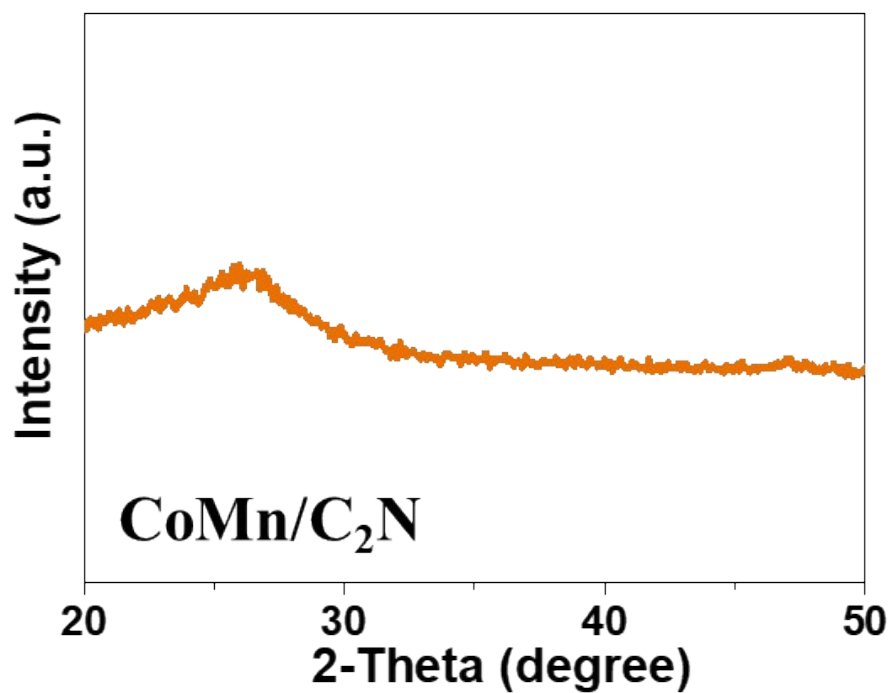
Figure S27. XRD pattern of CoMn/C$_2$N XRD pattern of CoMn/C$_2$N
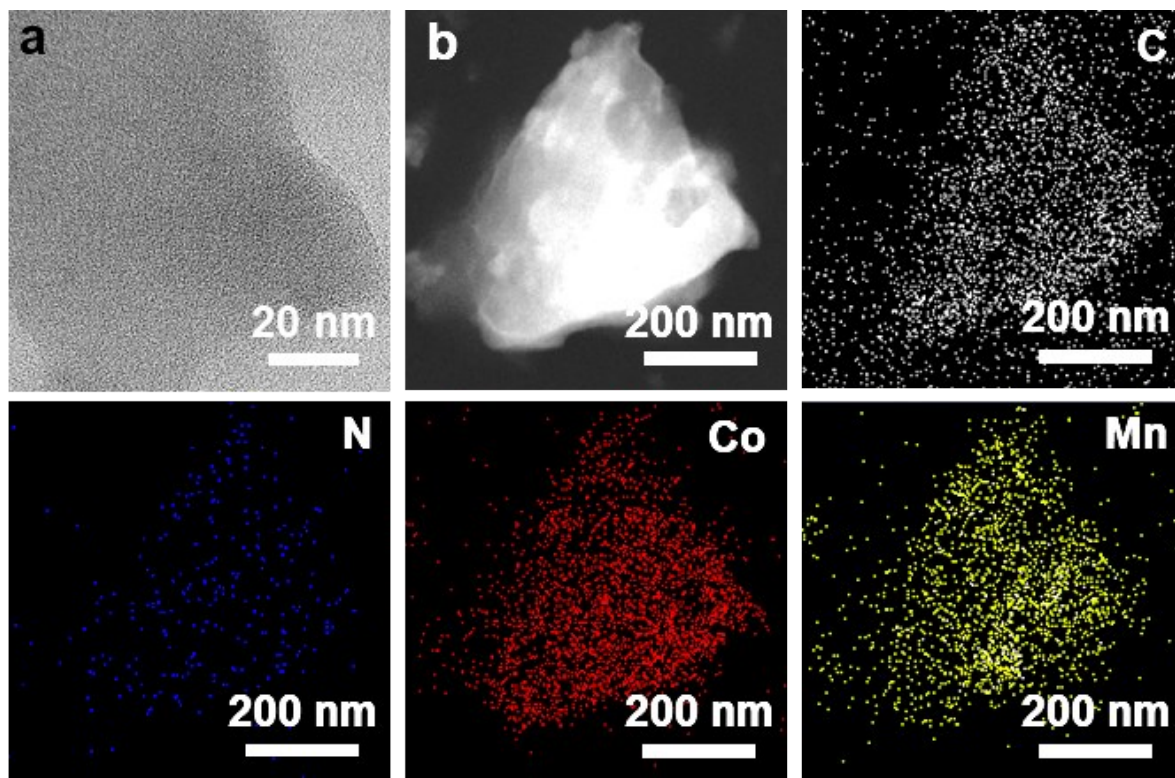
Figure S28. (a, b) TEM images and (c) EDS mapping data for CoMn/C$_2$N.
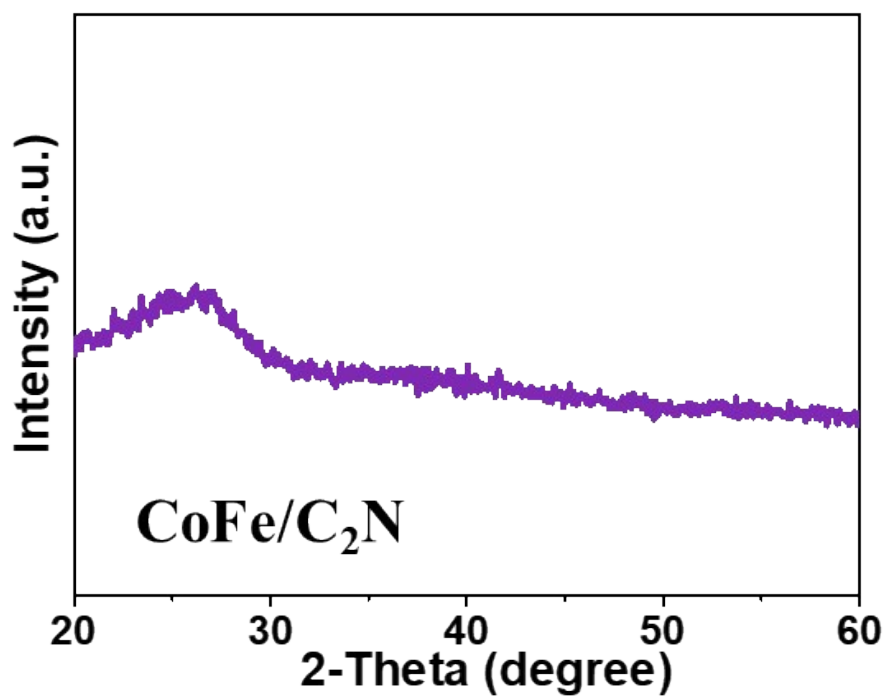
Figure S29. XRD pattern of CoFe/C$_2$N.

Table S1. Elemental quantiffication determined by different methods for C_2N, Co/C_2N-L, and Co/C_2N-H.

Sample	EDS (at.%)				EDS (wt.%)	TGA (wt.%)	ICP-OES (wt.%)
	C	N	O	Co	Co	Co	Co
C_2N	58.78	23.99	17.23	-	0	0	0
Co/C_2N-L	55.70	23.99	19.11	1.20	5.1	3.4	3.8
Co/C_2N-H	53.31	26.04	16.35	4.30	16.7	18.0	20.5

Table S2. Comparison of mass loading of metal elements in previously reported single atom catalysts and Co/C_2N.[8-21]

Sample	Method	Support	Mass loading (wt.%)	Reference
Co/C_2N-H	*C_2N based wet-chemistry*	*C_2N*	*20.5*	*This work*
Co-N-C@F127	ZIF based wet-chemistry	N doped carbon	6.2	8
Pt_1/BP_{defect}	Wet-chemistry	Carbon black	1.1	9
Fe-N-C-700	MgO based template-sacrificial approach with acid etching	N doped carbon	1.6	10
Co SAs/N-C	ZIF based wet-chemistry	N doped carbon	4	11
Co-N5/HNPCSs	SiO_2 based template-sacrificial approach with acid etching	Nitrogen doped carbon	3.54	12
Fe-SAs/NPS-HC	Polymer based coating approach	N doped carbon	1.54	13
$FeCl_1N_4$/CNS	Thermal-migrating method	N, S co-doped carbon	1.5	14
Co-N-C	$Mg(OH)_2$ based template-sacrificial approach with acid etching	N doped carbon	3.6	15
Fe-N_4 SAs/NPC	Wet-chemistry	polyphthalocyanine	1.96	16
NGM-Co	$Mg(OH)_2$ based template-sacrificial approach with acid etching	N doped carbon	1.23	17
FeNC-1000	Wet-chemistry	N doped carbon	3.3	18
ISA Fe/CN	ZIF based wet-chemistry	N doped carbon	2.16	19
Co, N-CNF-1000	ZIF based wet-chemistry	N doped carbon	2.52	20
Ir-NiO	Wet-chemistry	NiO	18	21

Table S3. EXAFS data fitting parameters of Co/C_2N-L and -H.

sample	Path	N	R (Å)	ΔE_0 (eV)	$\sigma^2(10^{-3}Å^2)$	Reduced chi-square	R factor
Co/C_2N-L	Co-N	1.9 ± 0.3	2.05 ± 0.02	3.8 ± 1.6	1.6 ± 2.7	94.1	0.007
	Co-C1	6.2 ± 0.7	2.17 ± 0.01	-3.1 ± 1.1	3.9 ± 1.6		
	Co-C2	1.7 ± 0.4	2.93 ± 0.03	10.0*	3.0*		
Co/C_2N-H	Co-N	2.0 ± 0.2	2.03 ± 0.01	7.0 ± 1.1	3.9 ± 2.0	354.3	0.007
	Co-C1	6.3 ± 0.4	2.15 ± 0.01	-3.0 ± 0.7	3.5 ± 0.9		
	Co-C2	1.0 ± 0.3	2.91 ± 0.03	10.0*	3.0*		

Table S4. Comparison of some recently reported pyrolysis-free COF-tailored ORR and OER electrocatalysts. Note: a: OER performance is measured in 0.1 M KOH; b: OER performance is measured in 1 M KOH.

Samples	ORR performance					OER performance		Bifunctionality (ORR+OER)	Reference
	n	V_{onset} (V)	$V_{1/2}$ (V)	j_L mA cm^{-2}	Tafel slope mV dec^{-1}	V_{10} (mV)	Tafel slope mV dec^{-1}		
Co/C$_2$N-H	3.91	0.89	0.72	5.9	65.5	369	69	Yes	This work
Cu-CTF/CP	-	0.91	~0.76	~5.2	-	-	-	No	*Angew. Chem. Int. Ed.* **2015**, 54, 11068
CTF-CSU1	2.6	0.79	0.57	5.6	-	-	-	No	*J. Catal.* **2018**, 362, 1
COP-P-SO$_3$-Co-rGO	3.7	0.88	~0.72	~4.4	67.4	-	-	No	*Angew. Chem. Int. Ed.* **2018**, 57, 12567
P-T/rGO	-	0.94	0.79	~3.8	70.4	-	-	No	*Angew. Chem. Int. Ed.* **2019**, 58, 11369
Co@TPA−PDI	3.9	0.91	~0.68	5.7	138	-	-	No	*ACS Appl. Mater. Interfaces* **2019**, 11, 5455
TAPA-OPE-gly	3.8	0.81	0.58	~4	-	-	-	No	*Chem. Eur. J.* **2020**, 26, 3810
JUC-528	3.8	-	0.7	5	65.9	-	-	No	*J. Am. Chem. Soc.* **2020**, 142, 81048108
CoCMP[a]	-	-	-	-	-	590	87	No	*Chem. Commun.* **2018**, 54, 4465
macro-COF-Co[a]	-	-	-	-	-	380	54	No	*J. Am. Chem. Soc.* **2019**, 141, 6623
Co$_{0.5}$V$_{0.5}$@COF-SO$_3$[b]	-	-	-	-	-	318	62	No	*J. Mater. Chem. A* **2020**, 8, 5907
C4-SHz COF[b]	-	-	-	-	-	320	39	No	*ACS Catal.* **2020**, 10, 5623

Table S5. Battery performance comparison of the Co/C$_2$N-based air cathode with previous reported single-atom-based air cathodes.[16-30]

Bifunctional air electrode	Discharge voltage @ 5 mAcm^{-2}	Power density mW cm^{-2}	Specific capacity, mAh g^{-1}	Durability		Reference
				cycle number@j, mA cm^{-2}	Time, h	
Co/C$_2$N-H	*1.30*	*220*	*742*	*6000@5mA*	*1000*	*This work*
Fe-N$_4$ SAs/NPC	NA	232	NA	108@2	36	16
FeCo-N$_x$-CN-30	1.26	150	NA	21@10	44	22
S-treated Fe/N/C	1.20	250	NA	120@5	20	23
CoN$_4$/NG	1.24	115	730	150@10	100	24
CoNi-SAs/NC	1.20	101	750	95@5	31	25
SCoNS	1.36	194	690	60@5	20	26
Fe-N$_x$-C	1.20	96.4	641	600@5	300	27
Co-N, B-CSs	0.9	100.4	NA	128@2	14	28
S, N-Fe/N/C-CNT	1.20	102.7	NA	100@5	NA	29
M-Fe-NCNS	NA	154.4	NA	1000@25	166	30

References

1. L. Trotochaud, S. L. Young, J. K. Ranney, and S. W. Boettcher, *J. Am. Chem. Soc.* 2014, **136**, 6744.

2. S. Hu, T. Han, C. Lin, W. Xiang, Y. Zhao, P. Gao, F. Du, X. Li and Y. Sun, *Adv. Funct. Mater.* 2017, **27**, 1700041.

3. G. Kresse and D. Joubert, *Phys. Rev. B*, 1999, **59**, 1758.

4. P. E. Blöchl, *Phys. Rev. B*, 1994, **50**, 17953.

5. J. P. Perdew, K. Burke and M. Ernzerhof, *Phys. Rev. Lett.*, 1996, **77**, 3865.

6. H. J. Monkhorst and J. D. Pack, *Phys. Rev. B*, 1976, **13**, 5188.

7. S. Grimme, J. Antony, S. Ehrlich and H. Krieg, *J. Chem. Phys.*, 2010, **132**, 154104.

8. Y. He, S. Hwang, D. A. Cullen, M. A. Uddin, L. Langhorst, B. Li, S. Karakalos, A. J. Kropf, E. C. Wegener, J. Sokolowski, M. Chen, D. Myers, D. Su, K. L. More, G. Wang, S. Litster and G. Wu, *Energy Environ. Sci.* 2019, **12**, 250-260.

9. J. Liu, M. Jiao, B. Mei, Y. Tong, Y. Li, M. Ruan, P. Song, G. Sun, L. Jiang, Y. Wang, Z. Jiang, L. Gu, Z. Zhou and W. Xu, *Angew. Chem.* 2019, **131**, 1175.

10. W. Liu, L. Zhang, X. Liu, X. Liu, X. Yang, S. Miao, W. Wang, A. Wang and T. Zhang, *J. Am. Chem. Soc.* 2017, **139**, 10790.

11. P. Yin, T. Yao, Y. Wu, L. Zheng, Y. Lin, W. Liu, H. Ju, J. Zhu, X. Hong, Z. Deng, G. Zhou, S. Wei and Y. Li, *Angew. Chem. Int. Ed.* 2016, **55**, 10800.

12. Y. Pan, R. Lin, Y. Chen, S. Liu, W. Zhu, X. Cao, W. Chen, K. Wu, W.-C. Cheong, Y. Wang, L. Zheng, J. Luo, Y. Lin, Y. Liu, C. Liu, J. Li, Q. Lu, X. Chen, D. Wang, Q. Peng, C. Chen and Y. Li, *J. Am. Chem. Soc.* 2018, **140**, 4218.

13. Y. Chen, S. Ji, S. Zhao, W. Chen, J. Dong, W.-C. Cheong, R. Shen, X. Wen, L. Zheng, A. I. Rykov, S. Cai, H. Tang, Z. Zhuang, C. Chen, Q. Peng, D. Wang and Y. Li, *Nat. Commun.* 2018, **9**, 5422.

14. Y. Han, Y. Wang, R. Xu, W. Chen, L. Zheng, A. Han, Y. Zhu, J. Zhang, H. Zhang, J. Luo, C. Chen, Q. Peng, D. Wang and Y. Li, *Energy Environ. Sci.* 2018, **11**, 2348.

15. W. Liu, L. Zhang, W. Yan, X. Liu, X. Yang, S. Miao, W. Wang, A. Wang and T. Zhang, *Chem. Sci.* 2016, **7**, 5758.

16. P. Yuan, L. Shoujie, S. Kaian, C. Xin, W. Bin, W. Konglin, C. Xing, C. Weng-Chon, S. Rongan, H. Aijuan, C. Zheng, Z. Lirong, L. Jun, L. Yan, L. Yunqi, W. Dingsheng, P.

Qing, Z. Qiang, C. Chen and L. Yadong, *Angew. Chem. Int. Ed.* 2018, **57**, 8614.

17. C. Tang, B. Wang, H.-F. Wang and Q. Zhang, *Adv. Mater.* 2017, **29**, 1703185.

18. G. Ren, L. Gao, C. Teng, Y. Li, H. Yang, J. Shui, X. Lu, Y. Zhu and L. Dai, *ACS Appl. Mater. Interfaces* 2018, **10**, 10778.

19. Y. Chen, S. Ji, Y. Wang, J. Dong, W. Chen, Z. Li, R. Shen, L. Zheng, Z. Zhuang, D. Wang and Y. Li, *Angew. Chem. Int. Ed.* 2017, **56**, 6937.

20. L. Shang, H. Yu, X. Huang, T. Bian, R. Shi, Y. Zhao, G. I. N. Waterhouse, L.-Z. Wu, C.-H. Tung and T. Zhang, *Adv. Mater.* 2016, **28**, 1668.

21. Q. Wang, X. Huang, Z. L. Zhao, M. Wang, B. Xiang, J. Li, Z. Feng, H. Xu and M. Gu, *J. Am. Chem. Soc.* 2020, DOI: https://doi.org/10.1021/jacs.9b12642.

22. L. Shuang, C. Chong, Z. Xiaojia, S. Johannes and T. Arne, *Angew. Chem. Int. Ed.* 2018, **57**, 1856.

23. Q. Wei, G. Zhang, X. Yang, Y. Fu, G. Yang, N. Chen, W. Chen and S. Sun, *J. Mater. Chem.* A 2018, **6**, 4605.

24. L. Yang, L. Shi, D. Wang, Y. Lv and D. Cao, *Nano Energy* 2018, **50**, 691.

25. X. Han, X. Ling, D. Yu, D. Xie, L. Li, S. Peng, C. Zhong, N. Zhao, Y. Deng and W. Hu, *Adv. Mater.* 2019, **31**, 1905622.

26. J. Wu, H. Zhou, Q. Li, M. Chen, J. Wan, N. Zhang, L. Xiong, S. Li, B. Y. Xia, G. Feng, M. Liu and L. Huang, *Adv. Energy Mater.* 2019, **9**, 1900149.

27. J. Han, X. Meng, L. Lu, J. Bian, Z. Li and C. Sun, *Adv. Funct. Mater.* 2019, **29**, 1808872.

28. Y. Guo, P. Yuan, J. Zhang, Y. Hu, I. S. Amiinu, X. Wang, J. Zhou, H. Xia, Z. Song, Q. Xu and S. Mu, *ACS Nano* 2018, **12**, 1894.

29. P. Chen, T. Zhou, L. Xing, K. Xu, Y. Tong, H. Xie, L. Zhang, W. Yan, W. Chu, C. Wu and Y. Xie, *Angew. Chem. Int. Ed.* 2017, **56**, 610.

30. M. Wang, H. Ji, S. Liu, H. Sun, J. Liu, C. Yan and T. Qian, *Chem. Eng. J.* 2020, **393**,

124702.